A spiral-windable, free-standing, durable membrane constructed with ultralong hydrogel@MnO2 nanowires for oil/water separation under harsh environment

Oluwaseun Ogunbiyi, Jayaprakash Saththasivam, Yongfeng Tong, Jenny Lawler, Zhaoyang Liu

Separation and Purification Technology 348 (2024) 127711

Contents lists available at ScienceDirect

Separation and Purification Technology

journal homepage: www.elsevier.com/locate/seppur

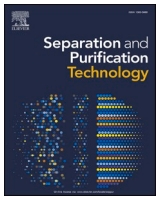

A spiral-windable, free-standing, durable membrane constructed with ultralong hydrogel@MnO_2 nanowires for oil/water separation under harsh environment

Oluwaseun Ogunbiyi, Jayaprakash Saththasivam, Yongfeng Tong, Jenny Lawler, Zhaoyang Liu*

Qatar Environment and Energy Research Institute (QEERI), Hamad Bin Khalifa University (HBKU), Qatar

ARTICLE INFO

Editor: Shujuan Zhang

Keywords:
Oily wastewater
Membrane
Spiral-windable
Free-standing
Durable

ABSTRACT

An ideal membrane for oil/water separation at industrial scale is expected to possess the combined merits of excellent separation performance, sound mechanical flexibility, and high durability under harsh environments. In response to these challenging requirements, we came up with a new concept to design the membrane constructed with ultralong hydrogel-functionalized MnO_2 nanowires. The super-oleophobic nanowires form highly open and tight pore structures within the membrane, which endows its high permeation flux (2800 L h^{-1} m^{-2} bar^{-1}), high oil/water separation efficiency (>99 %) and low fouling tendency for separating emulsified oil from water. Furthermore, the brittleness problem of MnO_2 materials is collectively resolved due to the high aspect ratio and surface functionalization of the hydrogel-functionalized MnO_2 nanowires. This results in the new membrane with extraordinary mechanical flexibility and potential for spiral-wound membrane modules, which are highly desired in industrial applications due to a lower footprint and lower capital cost. The new membrane also demonstrates high durability under harsh environments with non-neutral pH values or high salinities. Given its facile synthesis process and inexpensive materials, this spiral-windable and durable membrane with high separation performance has the great potential to be applied at industrial scale for oily wastewater treatment under harsh environments.

1. Introduction

Oil pollution remains a serious problem worldwide due to oil exploration and production activities that produce vast quantities of oily wastewater, which normally features high salt content and non-neutral pH values [1,2]. It is a necessary requirement to develop effective, low-cost technologies that can be used to treat this oily wastewater to achieve discharge compliance and protect marine environment [3]. Conventional technologies for oil/water separation, including hydrocyclone and air flotation, have quite a few limitations such as limited separation capability for small oil droplets and increased operating costs due to chemical additions [4]. Membrane filtration, using the mechanism of sieving effect, is commonly used for water treatment [5]. Previous studies showed membrane filtration is promising in separating emulsified oil from wastewater [6,7]. Polymeric membranes are dominating commercial market due to their low cost and ability to be used as spiral-wound module with rolled-up membranes [8]. However, most of them suffer from membrane fouling and permeation flux reduction, which are caused by their oleophilic materials and segregated pore structures, respectively [9]. Ceramic membranes are well known for their unique hydrophilicity and oleophobicity, making them a preferred choice for oil/water separation [10]. However, the poor mechanical flexibility excludes them from spiral-wound modules. Among most industrial applications, spiral-wound modules are highly desired due to the benefits of reduced footprints and capital cost for water treatment plants [11]. Conventional membranes are normally composed of two layers, with a selective layer on top of a support layer [12]. However, the support layer could adversely affect the membrane performance, which is caused by the issues of internal concentration polarization and fouling occurring inside the support layer [13]. Free-standing membrane without support layers is a quest to mitigate these issues [14]. The methods to fabricate spiral windable, free-standing, high-performance, and low-fouling membranes for treating oily wastewater is greatly in demand.

Previous studies showed a great deal of effort has been put to develop

* Corresponding author.
E-mail address: zhliu@hbku.edu.qa (Z. Liu).

https://doi.org/10.1016/j.seppur.2024.127711
Received 20 February 2024; Received in revised form 16 April 2024; Accepted 25 April 2024
Available online 3 May 2024

new membranes with high separation performance, high flexibility, and low fouling tendency. The nature of fish scales has inspired the fabrication of membranes with superoleophobic and low-fouling surfaces [15,16]. One of the studies involved the fabrication of a hydrogel-coated mesh structure that exhibited unique superoleophobicity under water for the separation of oily water mixtures [17]. Nevertheless, these filters have been known to suffer from the low separation rate for emulsified oils, due to their large pore size in the mesh substrates [18]. In another study, an ultrathin hydrogel selective layer was coated on a phase-inversion-made membrane substrate, which demonstrated high anti-fouling property for separating oil/water emulsion [19]. However, the membrane faced the problem of relatively low water flux due to its segregated pore structure formed by phase inversion method. Electrospinning technique has been explored for fabricating nonwoven fibrous membranes, because of its merit with interconnected porous structure that leads to high water flux [20]. However, the disadvantages of this technique include a relatively bigger pore size distribution and unwanted macrovoids caused by static electric repulsion, which ultimately compromised the membrane selectivity [21]. These factors all contribute to the limited potential and utilization of these previous membranes for practical and industrial applications. Recently, Manganese dioxide (MnO_2) nanowires have emerged as ideal building block for filtration membranes, due to their unique physical and chemical properties and nanostructured morphology, distinguishing them from bulk MnO_2 [22]. They feature high aspect ratios, typically with nanometer-scale diameters and micrometer-scale lengths. With flexibility and mechanical resilience, these nanowires can withstand bending and deformation, making them applicable in various application fields. However, they are vulnerable to extreme environmental conditions, such as surface hydrolysis reactions that increase their dissolution in acidic or alkaline solutions [23]. Despite their previous usage in oil absorption [24] or filtration [25], there are still some knowledge gaps in the research addressing their susceptibility to extreme environmental conditions through effective surface modifications.

In this work, we proposed a new concept for developing spiral windable, free-standing and durable membranes with high oil/water separation performance. The ultralong, superoleophobic and corrosion-resistant hydrogel-functionalized MnO_2 nanowires were used as the building blocks for the new membrane. The membrane exhibits a high efficiency for separating emulsified oil from water due to its tight and nanoporous structure, as well as high water flux attributed to its open and three-dimensionally-interconnected pore structure. Notably, its excellent durability was displayed under harsh environments with high water salinities or non-neutral pH values. In contrast to the ceramic nature of pristine MnO_2 nanowires, the new free-standing membrane constructed with ultralong hydrogel-functionalized MnO_2 nanowires shows extraordinary mechanical flexibility and ability for spiral-wound module. These combined advantages make the new membrane highly advantageous for oily wastewater treatment at industrial scale.

2. Materials and methods

2.1. Chemicals and equipment

The chemicals that were used in this research were manganese sulfate monohydrate ($MnSO_4{\cdot}H_2O$), ammonium persulfate (APS) and ammonium sulfate ($(NH_4)_2SO_4$), hydrochloric acid, sodium hydroxide, sodium dodecyl sulfate and Poly (vinyl alcohol) (PVA) (M.W. = 60,000, 99 % purity) and glutaraldehyde (aqueous solution, 50 wt%) were purchased from Sigma-Aldrich. Sunflower oil, n-hexane, n-octane, and engine oil were used to reproduce emulsified oil, while sea salt was used to simulate and prepare highly saline water. The oil and the sea salt were sourced locally. A JORIN-ViPA B HiFlow visual process analyzer was used to measure the oil droplet size distributions.

2.2. Synthesis of ultralong MnO_2 nanowires

The ultralong MnO_2 nanowires have been successfully synthesized using a simple hydrothermal method. In a typical process, 4 g Manganese sulfate monohydrate ($MnSO_4{\cdot}H_2O$), 5.2 g ammonium persulfate (APS) and 10 g ammonium sulfate ($(NH_4)_2SO_4$) were dissolved in 100 ml distilled water. The solution was stirred for a total of 5 min. The mixture was then transferred to a 60 ml Teflon-lined stainless-steel autoclave, sealed, and maintained at 220 °C for 96 h in an electric oven. This was then removed carefully and allowed to cool down to room temperature in air. A brown precipitate was collected and washed with distilled water and ethanol several times to remove any impurities.

2.3. Preparation of free-standing MnO_2 nanowire membrane

1 g of MnO_2 nanowire was dissolved in 100 ml of distilled water and immersed in a sonication bath to produce a homogeneous suspension. This was then filtered under a vacuum and passed through a glass fiber filter of 0.45 μm, then it was dried at 60 °C for around 10 min. A MnO_2 nanowire membrane was then manually removed from the glass fiber substrate. The membrane thicknesses could be varied by changing the weight percentage of MnO_2 nanowires in the solutions for membrane deposition

2.4. Functionalization of MnO_2 nanowire with PVA hydrogel

A thin PVA functional layer was prepared using the solution casting method. The first step involved preparing an aqueous 1 % (w/w) PVA solution by dissolving PVA in distilled water at 90 °C and was continuously stirred. After cooling down to room temperature, glutaraldehyde was added to the polymer solution with glutaraldehyde/PVA mass ratio of 0.005. The resulting PVA solution was then transferred onto a pre-made MnO_2 nanowire membrane under vacuum condition. The PVA-deposited membranes were dried for crosslinking at 50 °C for 2 h. After drying, the deposited membrane was easily removed from the glass fiber by peeling it off.

2.5. Preparation of oil-in-water emulsion

Oil-in-water emulsions were prepared in a sonication bath by mixing 90 ml of distilled water and 10 ml of different oils for 5 min. These include sunflower oil, n-hexane, n-octane, and engine oil. The homogeneous white-colour solutions were subsequently diluted to 1 L of distilled water. The oil-in-water emulsions were stable for a sustained period of time (30 days) under ambient conditions. The emulsion feed salinity ranged from around 300 ppm to 45,000 ppm using sodium chloride. The oil–water emulsion has a mean droplet size of 3.61 μm as shown in Fig. S1.

2.6. Characterization

Several techniques were used to characterize the samples to determine their structural and physicochemical features. Powder X-ray diffraction (XRD) was used to determine the phase composition of the synthesized nanowires. The findings were recorded using a Bruker D8 Advance (Bruker, Germany) using CuK radiation () 1.540 59) at a step size of 0.02° and a scan rate of 0.05°/min in the 2 range between 2° and 90°. The standard Thermal-fisher ESCALAB 250XI type XSP platform was used for the X-ray Photoelectron Spectroscopy (XPS) analysis. A monochromatic Al Kα Anode X-ray beam was utilized with a photon energy of 1486.8 eV and an incident angle of 45° to the sample surface. All the spectra obtained were calibrated to the C–C peak at 284.8 eV in the C1s reference. The chemical composition and surface morphology of the material were investigated using a field emission scanning electron microscope (FE-SEM, QUANTA FEG 650, Thermo Fisher Scientific, USA) with energy dispersive spectroscopy (EDS, Bruker Xflash 6l60,

Germany) for elemental analysis, and cross-sectional SEM images of the membranes to measure coating thickness. To assess the hydrophilicity of the produced material, contact angle measurements were acquired using an advanced goniometer (Rame-hart A100, USA) via a sessile drop method. The total organic carbon (TOC) analyzer (Shimadzu, TOC-L, Japan) was used to determine the concentration of oil in the feed and filtrate samples. The pore size distribution of the membranes was measured using the equipment of Porometer 3Gzh (Quantachrome).

2.7. Performance test for oil/water separation

The membrane performance was assessed using vacuum filtration apparatus that has an effective membrane area of 17.4 cm^2. All filtration experiments were carried out under a pressure of 50 kPa using a diaphragm vacuum pump. Oil rejection rates were calculated using the differences in the TOC values of the feed and permeate. Membrane flux was calculated using the permeation volume obtained over a fixed filtration period. To investigate the stability of the nanowire membrane in harsh environment, the membrane was immersed in various pH solutions (pH = 2, 4, 6, 8, 10, and 12) and different salinities at room temperature for 7 days before conducting the performance test for oil/water separation.

3. Results and discussions

Fine and ultralong MnO_2 nanowires were synthesized using a facile and one-pot hydrothermal method. The vacuum filtration method was used to fabricate the MnO_2 nanowire membranes. Poly (vinyl alcohol) is a semi-crystalline, water-soluble polymer with high mechanical capability, chemical resistance, and oleophobicity [26]. To improve flexibility and durability, PVA hydrogel was coated and cross-linked onto the surfaces of MnO_2 nanowire membranes (experimental details are presented in Fig. 1).

The investigation of the crystalline structures and phase purity of the nanowire membranes were carried out using X-ray diffraction (XRD). The XRD arrangement of the fabricated free-standing MnO_2 nanowire membrane can be seen in Fig. 2. All of the peaks indicate a tetragonal α-MnO_2 (space group: I4/m) with cell parameters a = 9.78 Å and c = 2.86 Å, which are in line with the standard card (PDF 81-1947) peak values. There is no other impurity present within the sample, as shown in Fig. 2.

The optical views in Fig. 3 show the colors of the membrane samples slightly turned from dark brown to light brown, after the PVA hydrogel layer was coated on the pristine MnO_2 nanowire membranes. The morphology and microstructure of the membranes were studied using scanning electron microscopy (SEM). The SEM images in Fig. 3a show a highly porous network of the membrane constructed by ultralong and interwoven MnO_2 nanowires. It is crucially noticeable that the lengths of the MnO_2 nanowires range from tens to hundreds of micrometers and the diameters range from 20 to 50 nm, indicating a high aspect ratio that

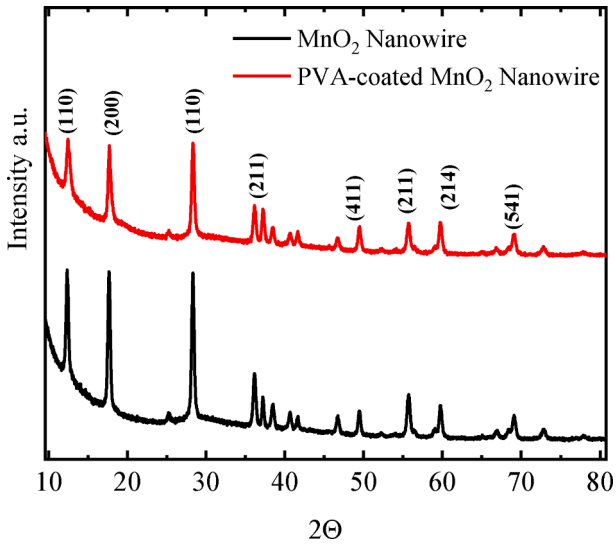

Fig. 2. XRD spectra of the MnO_2 nanowire membranes with and without PVA coating. The major peaks show the presence of MnO_2 materials within the fabricated membranes.

favors the formation of an integrated membrane. The transparent and thin PVA hydrogel layers are homogeneously interpenetrated into the network structure with close contacts to the MnO_2 nanowires, which were then assembled into bundles (Fig. 3b). Cracks were observed on the pristine MnO_2 nanowire membranes when folded (Fig. S2). This is due to the MnO_2 nanowires exhibiting a bit of ceramic nature. To overcome this fragility issue, the thin layers of the PVA hydrogel were coated on the MnO_2 nanowires. Fig. 3c shows an optical image of the PVA hydrogel-functionalized MnO_2 nanowire membrane, from which the free-standing membrane was spirally wound without any cracks, suggesting excellent mechanical flexibility and integrity of the membrane. It was found that the top surface mean pore sizes decreased from 0.09 μm to 0.07 with 1 w/w % PVA hydrogel coating on MnO_2 nanowire membranes. This was measured using pore size analyzer (porometer 3Gzh), as shown in Fig. S3. When the PVA concentration reached 2 w/w %, the pores of the nanowire membranes became partially blocked, as shown in Fig. S4. This interconnected porous network of the new membrane could allow for easier water permeability due to less resistance, and at the same time the tight nano-sized pores could enable its effective rejection of small oil droplets.

Fig. 4 shows the comparison of three mno$_2$ samples with different PVA coating content (0 %, 1 % and 2 %), with the survey spectra in (a) and Mn2p, O1s and C1s (b-d), respectively. The Survey spectra in Fig. 4 (a) indicates the very clean sample with only Mn2p, C1s and O1s being observed. The difference with PVA coating lies mainly in the C1s and

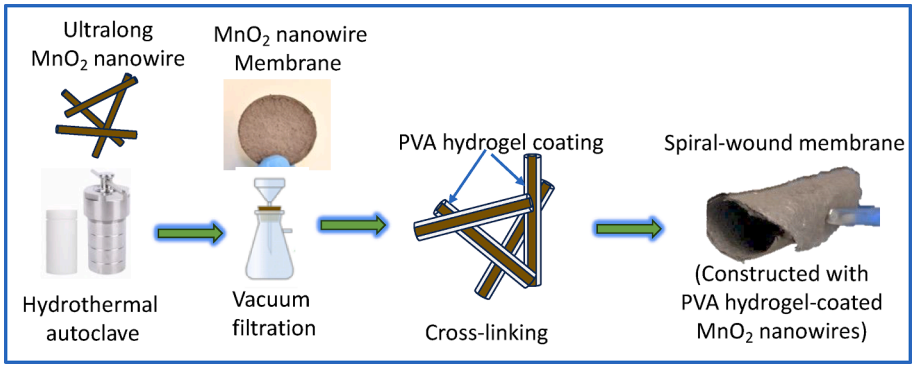

Fig. 1. Schematic diagram showing the fabrication methodology of flexible and free-standing membranes constructed with ultralong PVA hydrogel-functionalized MnO_2 nanowires.

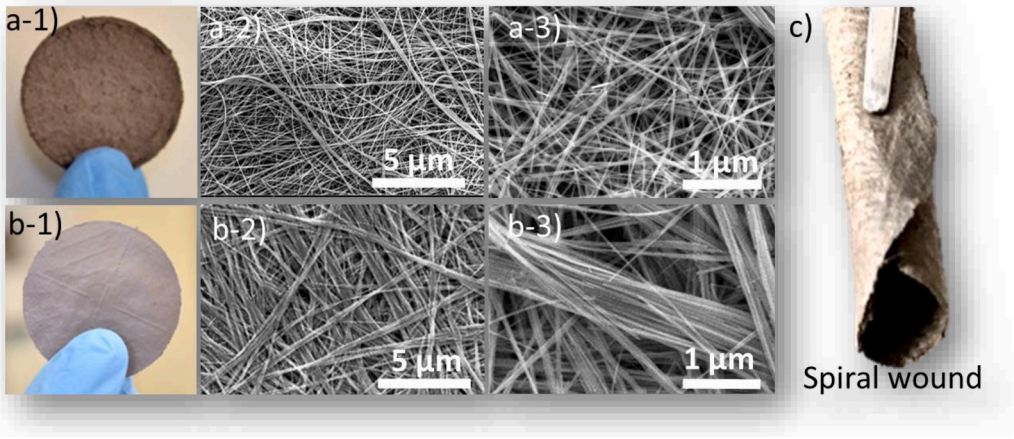

Fig. 3. (A) Pristine MnO_2 nanowire membranes: (a-1) optical image of the membrane. (a-2) low-magnification SEM image of the membrane composed of ultralong MnO_2 nanowires. (a-3) high-magnification SEM image of the membrane showing interconnected and tight network structure. (B) PVA hydrogel-functionalized MnO_2 nanowire membrane: (b-1) optical image of the membrane. (b-2) low-magnification SEM image of the membrane showing highly porous network of the membrane. (b-3) high-magnification SEM image of the membrane showing nanowire bundles. (C) The photo demonstrates the high flexibility of PVA hydrogel-functionalized MnO_2 nanowire membrane, which can be assembled as a spiral wound module that is highly desired in industrial applications.

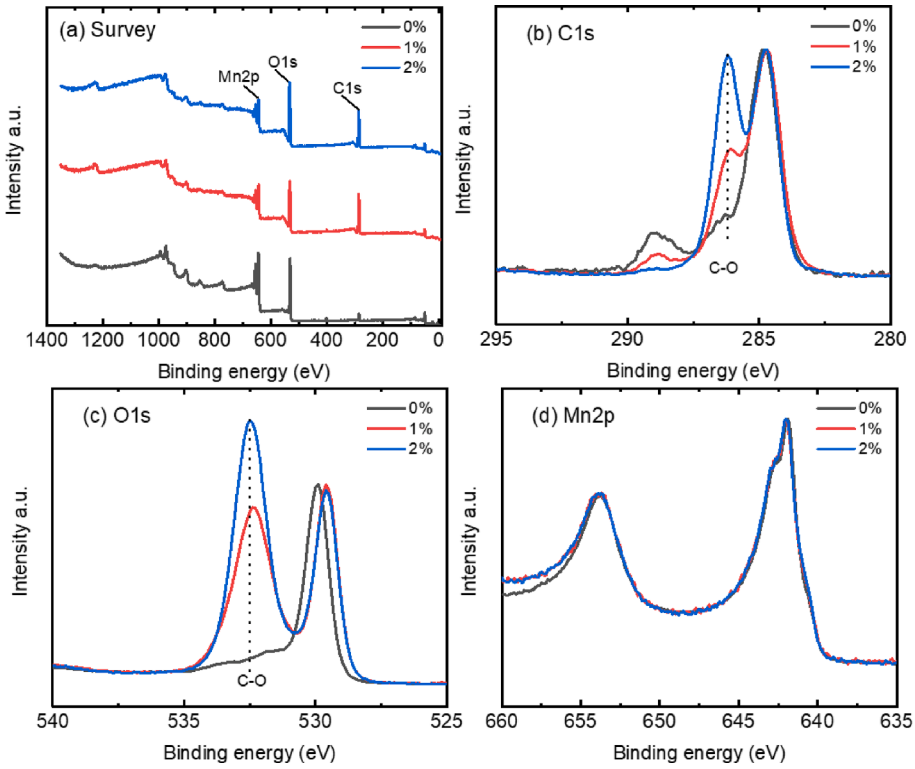

Fig. 4. The comparison of core levels (a) survey, (b) the C1s, (c) the O1s and (d) the Mn2p for MnO_2 nanowire membranes with different PVA coating contents (0 %–2%).

O1s profile, where we can find a C-O bond increase at 286.1 eV in C1s in Fig. 4 (b) as well as at 532.3 eV in the O1s spectrum in Fig. 4(c). It's worth noting that the Mn2p in Fig. 4(d) presents no clear variation, indicting the structure integration with the PVA coating. A detailed deconvolution of the core levels is given in Fig. S5 in the supporting information. Briefly, the Mn2p presents the typical MnO_2 profile with Mn2+, Mn3+ and Mn4+ state and the O1s shows the Mn-O, the Mn-OH from the MnO_2 nanofibers and the C-O bond from the PVA coating.

As shown in Fig. 5 (a), the water contact angle on the PVA hydrogel-functionalized MnO2 nanowire membranes was 0°, showing the membrane's super-hydrophilicity. The membrane also shows super-oleophobic properties as shown in Fig. 5 (b). Additionally, Fig. 5 (c) showcases rapid water penetration (within one second) into MnO_2 nanowire membranes with (black) and without (red) PVA hydrogel functionalization, implying a swift mass transfer rate of aqueous-based solutions. This is attributed to the unique properties of the new membranes, including their 3-D interconnected porous structure formed by intertwined nanowire substrates and super-hydrophilic surfaces.

The membrane thickness can be adjusted by varying the amount of MnO_2 nanowire in the stock solutions used for membrane preparation. The thickness increased with a higher amount of MnO_2 nanowires in the stock solution. The thickness of the membrane was measured using SEM

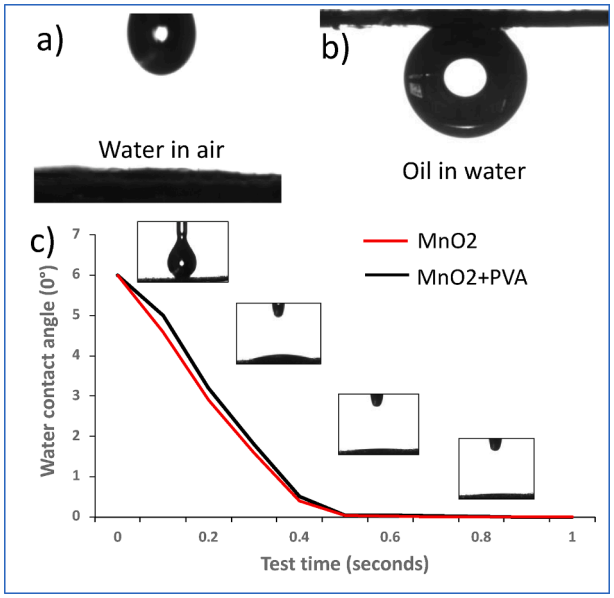

Fig. 5. Wettability study for MnO_2 nanowire membranes. Microscopic images of (a) Water contact angle (0°), revealing super-hydrophilicity of the membranes. (b) Underwater oil contact angle (153 ± 1.5°), indicating the high oleophobicity of the membranes. (c) Dynamic water contact angles, showing water droplet behavior on the MnO_2 nanowire membranes with (black) and without (red) PVA hydrogel functionalization.

cross-section images as shown in Fig. 6 (a). Water permeation flux and the rate of oil rejection as a function of membrane thickness is highlighted in Fig. 6 (b). As thickness of the membrane increased from 4 μm to 10 μm, the oil rejection rate of the membranes significantly increased from 95 % to over 99 %, and reached a plateau even after the thickness was increased further from 10 μm to 12 μm. However, the water flux of the membranes decreased from 4600 L/m^2.h.bar and 2000 L/m^2.h.bar as the membrane thickness increased. The criteria for optimized membrane thickness were set based on the highest oil rejection rate. Therefore, the membrane thickness of 10 μm was chosen as the optimized membrane thickness, where the oil rejection rate was >99 % and the water flux was as high as 2800 L/m^2.h.bar. To investigate the mechanical strength of the membrane, the membrane's performance in terms of water flux and oil rejection was assessed by subjecting it to multiple folding, as illustrated in Fig. S6. The consistent performance observed under these conditions indicates the durability of the membrane and its suitability for practical applications. Traditional ceramic membranes often face challenges due to mechanical brittleness [27,28], which can lead to reliability issues and susceptibility to damage, particularly under harsh conditions [29,30]. This challenge was effectively mitigated in this study by utilizing ultralong MnO_2 nanowires as the building block and by surface modification with PVA hydrogel for the membranes.

The membranes were tested against different types of emulsified oil, namely sunflower oil, n-hexane, n-octane, and engine oil. Their performance in terms of oil rejection ratio and water flux are shown in Fig. 7. The oil rejection rates were >99 % for all the different oils. The high oil rejection rates were achieved using the sieving effect as the membranes' pore size is finer than the emulsified oil droplets. These oil droplets are usually 2 to 5 μm (d_{90} = 5.96 μm) in size as shown in Fig. S1. Commercial polymeric microfiltration (MF) and ultrafiltration (UF) membranes can attain elevated rates of oil rejection due to their submicron pore dimensions. However, these membranes experience reduced water flux and are susceptible to swift fouling by oil. In our investigation, significantly higher water fluxes were achieved, ranging from 2800 L/(m^2.h.bar) to 2950 L/(m^2.h.bar), when compared to a commercial membrane. These results can be partially explained using the dynamic water contact angle measurements shown in Fig. 5C wherein, the water droplet rapidly penetrated into the membranes within 1 s. The high water flux was achieved due to the superhydrophilicity and interconnected porous structure for the nanowire membranes as evidenced in Fig. S8.

During continuous operation, the membranes were assessed for water flux and oil rejection rate. Fig. 8 illustrates that the membranes consistently maintained an oil rejection rate >99 % throughout. Moreover, the flux remained stable, averaging at 2800 L/(m^2·h·bar). This consistent performance indicates the membrane's resistance to irreversible fouling. Additionally, in Fig. 5b, the oil contact angle exceeded 150°, demonstrating the membrane's underwater superoleophobicity, which prevents firm adherence of oil droplets to the membrane surface. This property facilitates easy removal of reversible oil fouling. Furthermore, between filtration cycles, the membranes were washed with 50 ml of hot water (50 °C) to remove any residual oil, eliminating the need for chemicals. This feature presents an advantage over conventional membranes, which often require chemical cleaning, leading to secondary environmental pollution.

A huge amount of oily wastewater is generated from oil production and transportation sectors. This wastewater often contains high salinities and is in the non-neutral pH range. These extreme environments create challenges for membranes' operation. This study assessed the durability of the membranes by examining alterations in their performance following immersion in solutions with a pH range of 2 to 12 for a duration of 7 days. Afterwards, the membrane performance was evaluated using the same membrane sample to test their performance. The excellent pH stability of the hydrogel-functionalized MnO_2 nanowire membranes was shown in Fig. 9a with consistent oil rejection rates. However, a drastic reduction in oil rejection for the pristine MnO_2 nanowire membrane was observed (data not shown here). The pristine

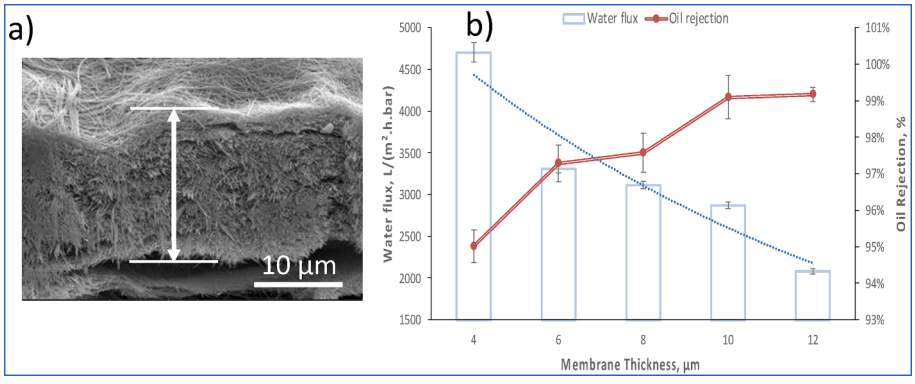

Fig. 6. (a) SEM image showing a cross-sectional view of the PVA hydrogel-functionalized MnO_2 nanowire membrane. (b) The performances of the membrane were tested with water flux and oil rejection as a function of the thickness of the membrane.

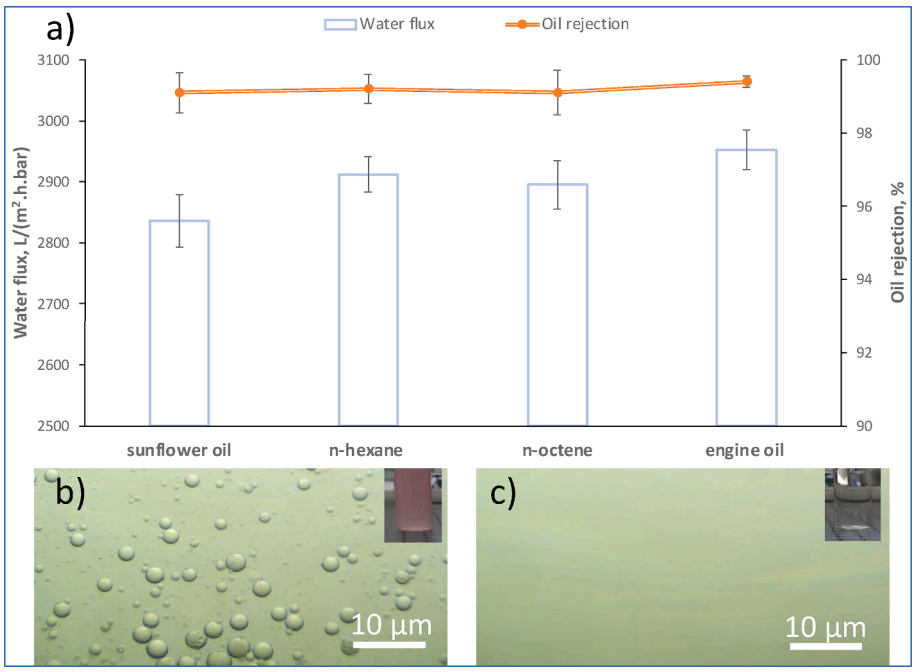

Fig. 7. (a) Performance tests of water flux and oil rejection rate for the new membranes were conducted with different types of emulsified oil. Microscopy images of emulsified oil-in-water solutions before (b) and after (c) membrane filtration. The inserted photographs show the solutions stained with red dye to highlight the effective oil removal after treatment.

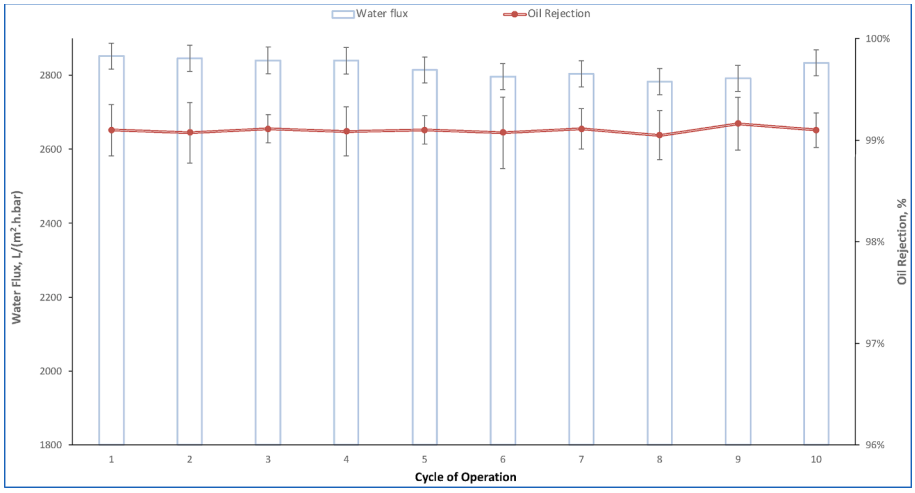

Fig. 8. Anti-fouling performance of the hydrogel-functionalized MnO_2 nanowire membrane over continuous operation.

MnO_2 nanowire membrane was noticeably damaged. Mn^{3+} is unstable at pH < 9 due to the disproportionation reaction [31]. The good pH stability of the hydrogel-functionalized MnO_2 nanowire membranes could be ascribed to the protection from the cross-linked PVA coating layers, which has excellent stability over a wide range of pH values. The effect of salinities on oil removal were also investigated. As shown in Fig. 9b, oil removal efficiencies were not changed at various levels of salinity, hence indicating the stability of the membrane. Consistent oil removal efficiencies across different salinity levels could be attributed to two primary factors. Firstly, the solubility of oil in water is generally low, regardless of salinity levels. Therefore, changes in salinity may not have a significant impact on the solubility of oil, and thus the effectiveness of oil removal processes may remain consistent. Secondly, membrane filtration relies on the size exclusion of the membrane to separate oil droplets from water. This membrane's pore size is much smaller than oil droplets, which leads to relatively constant oil rejection rates across different salinity levels.

4. Conclusion

A spiral-windable and freestanding membrane consisting of ultralong hydrogel-functionalized MnO_2 nanowires have successfully been fabricated using facile method. The ultralong 1D nanowires and the uniform hydrogel coating collectively endows the membrane with high flexibility, enabling its use as a spiral wound module, which is a significant advantage for industrial applications. The highly open and nanoporous network structure of the membrane provides excellent oil/water separating performance in terms of water flux and oil rejection rate. The functionalization of the membrane with PVA hydrogel layer provides excellent reusability due to its super-oleophobicity, and particularly high durability due to its corrosion resistance under harsh environments. The membrane can deliver a consistently high water flux

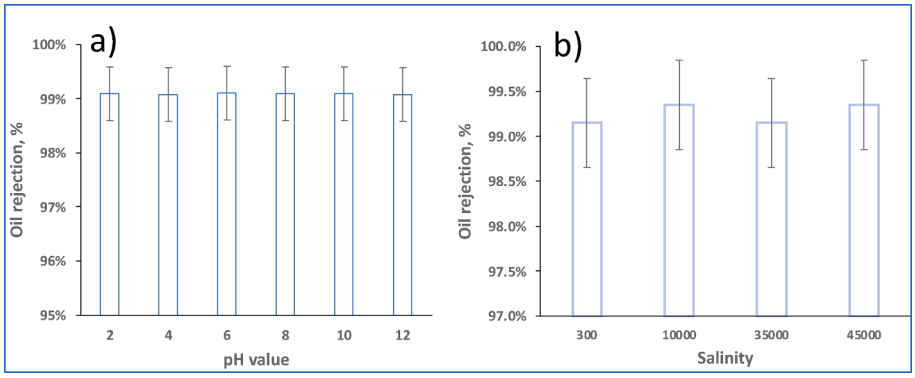

Fig. 9. Durability test of the hydrogel-functionalized MnO_2 nanowire membranes under harsh environmental conditions (a) different pH values in the solutions and (b) different salinities in the solutions.

of 2800 LMH/bar and oil rejection of >99 % after continuous operation. Given its facile synthesis process and inexpensive materials, the new membrane holds great potential for oily wastewater treatment at industrial scale.

CRediT authorship contribution statement

Oluwaseun Ogunbiyi: Writing – original draft, Methodology, Investigation, Funding acquisition, Formal analysis, Conceptualization. **Jayaprakash Saththasivam:** Writing – review & editing, Methodology, Formal analysis. **Yongfeng Tong:** Writing – original draft, Methodology. **Jenny Lawler:** Writing – review & editing, Investigation, Funding acquisition. **Zhaoyang Liu:** Writing – original draft, Methodology, Investigation, Funding acquisition, Formal analysis, Conceptualization.

Declaration of competing interest

The authors declare that they have no known competing financial interests or personal relationships that could have appeared to influence the work reported in this paper.

Data availability

Data will be made available on request.

Acknowledgement

Thank Qatar National Library (QNL) for funding support for the publication.

Appendix A. Supplementary material

Supplementary data to this article can be found online at https://doi.org/10.1016/j.seppur.2024.127711.

References

[1] T.S. Alomar, B.H. Hameed, M. Usman, F.A. Almomani, M.M. Ba-Abbad, M. Khraisheh, Recent advances on the treatment of oil fields produced water by adsorption and advanced oxidation processes, J. Water Process Eng. 49 (2022) 103034, https://doi.org/10.1016/j.jwpe.2022.103034.
[2] R. Elshorafa, J. Saththasivam, Z. Liu, S. Ahzi, Efficient oil/saltwater separation using a highly permeable and fouling-resistant all-inorganic nanocomposite membrane, Environ. Sci. Pollut. Res. 27 (2020) 15488–15497, https://doi.org/10.1007/s11356-020-08021-x.
[3] K. Wang, W. Yiming, J. Saththasivam, Z. Liu, A flexible, robust and antifouling asymmetric membrane based on ultra-long ceramic/polymeric fibers for high-efficiency separation of oil/water emulsions, Nanoscale 9 (2017) 9018–9025, https://doi.org/10.1039/C7NR02364B.
[4] J. Saththasivam, O. Ogunbiyi, J. Lawler, R. Al-Rewaily, Z. Liu, Evaluating dissolved air flotation for oil/water separation using a hybridized coagulant of ferric chloride and chitosan, J. Water Process Eng. 47 (2022) 102836, https://doi.org/10.1016/j.jwpe.2022.102836.
[5] Y. Zhu, W. Xie, S. Gao, F. Zhang, W. Zhang, Z. Liu, J. Jin, Single-walled carbon nanotube film supported nanofiltration membrane with a nearly 10 nm thick polyamide selective layer for high-flux and high-rejection desalination, Small 12 (2016) 5034–5041, https://doi.org/10.1002/smll.201601253.
[6] P. Gao, Z. Liu, D.D. Sun, W.J. Ng, The efficient separation of surfactant-stabilized oil–water emulsions with a flexible and superhydrophilic graphene–TiO2 composite membrane, J. Mater. Chem. A 2 (2014) 14082–14088, https://doi.org/10.1039/C4TA02039A.
[7] M. Padaki, R. Surya Murali, M.S. Abdullah, N. Misdan, A. Moslehyani, M.A. Kassim, N. Hilal, A.F. Ismail, Membrane technology enhancement in oil–water separation. A review, Desalination 357 (2015) 197–207, https://doi.org/10.1016/j.desal.2014.11.023.
[8] M.M. Pendergast, E.M.V. Hoek, A review of water treatment membrane nanotechnologies, Energy Environ. Sci. 4 (2011) 1946–1971, https://doi.org/10.1039/C0EE00541J.
[9] P.D. Sutrisna, K.A. Kurnia, U.W.R. Siagian, S. Ismadji, I.G. Wenten, Membrane fouling and fouling mitigation in oil–water separation: a review, J. Environ. Chem. Eng. 10 (2022) 107532, https://doi.org/10.1016/j.jece.2022.107532.
[10] J. Usman, M.H.D. Othman, A.F. Ismail, M.A. Rahman, J. Jaafar, Y.O. Raji, A. O. Gbadamosi, T.H. El Badawy, K.A.M. Said, An overview of superhydrophobic ceramic membrane surface modification for oil-water separation, J. Mater. Res. Technol. 12 (2021) 643–667, https://doi.org/10.1016/j.jmrt.2021.02.068.
[11] S.S. Bucs, N. Farhat, J.C. Kruithof, C. Picioreanu, M.C.M. van Loosdrecht, J. S. Vrouwenvelder, Review on strategies for biofouling mitigation in spiral wound membrane systems, Desalination 434 (2018) 189–197, https://doi.org/10.1016/j.desal.2018.01.023.
[12] H. Mokarizadeh, S. Moayedfard, M.S. Maleh, S.I.G.P. Mohamed, S. Nejati, M. R. Esfahani, The role of support layer properties on the fabrication and performance of thin-film composite membranes: the significance of selective layer-support layer connectivity, Sep. Purif. Technol. 278 (2021) 119451, https://doi.org/10.1016/j.seppur.2021.119451.
[13] X. Lu, L.H. Arias Chavez, S. Romero-Vargas Castrillón, J. Ma, M. Elimelech, Influence of active layer and support layer surface structures on organic fouling propensity of thin-film composite forward osmosis membranes, Environ. Sci. Technol. 49 (2015) 1436–1444, https://doi.org/10.1021/es5044062.
[14] W. Ma, M. Zhang, Z. Liu, C. Huang, G. Fu, Nature-inspired creation of a robust free-standing electrospun nanofibrous membrane for efficient oil–water separation, Environ. Sci. Nano 5 (2018) 2909–2920, https://doi.org/10.1039/C8EN00895G.
[15] J. Zhang, L. Wu, Y. Zhang, A. Wang, Mussel and fish scale-inspired underwater superoleophobic kapok membranes for continuous and simultaneous removal of insoluble oils and soluble dyes in water, J. Mater. Chem. A 3 (2015) 18475–18482, https://doi.org/10.1039/C5TA04839G.
[16] Y. Lv, X. Xi, L. Dai, S. Tong, Z. Chen, Hydrogel as a superwetting surface design material for oil/water separation: a review, Adv. Mater. Interfaces 8 (2021) 2002030, https://doi.org/10.1002/admi.202002030.
[17] Y.-Q. Liu, Y.-L. Zhang, X.-Y. Fu, H.-B. Sun, Bioinspired underwater superoleophobic membrane based on a graphene oxide coated wire mesh for efficient oil/water separation, ACS Appl. Mater. Interf. 7 (2015) 20930–20936, https://doi.org/10.1021/acsami.5b06326.
[18] Y. Peng, G. Wen, X. Gou, Z. Guo, Bioinspired fish-scale-like stainless steel surfaces with robust underwater anti-crude-oil-fouling and self-cleaning properties, Sep. Purif. Technol. 202 (2018) 111–118, https://doi.org/10.1016/j.seppur.2018.03.035.
[19] D. Qin, Z. Liu, H. Bai, X. Song, Z. Li, D.D. Sun, Fine-tuning selective layer architecture of hydrogel membrane towards high separation performances for engineered osmosis, J. Membr. Sci. 592 (2019) 117370, https://doi.org/10.1016/j.memsci.2019.117370.
[20] H. Meng, T. Xu, M. Gao, J. Bai, C. Li, An oil-contamination-resistant PVP/PAN electrospinning membrane for high-efficient oil–water mixture and emulsion separation, J. Appl. Polym. Sci. 138 (2021) 50043, https://doi.org/10.1002/app.50043.

[21] X. Yan, X. Xiao, C. Au, S. Mathur, L. Huang, Y. Wang, Z. Zhang, Z. Zhu, M.J. Kipper, J. Tang, J. Chen, Electrospinning nanofibers and nanomembranes for oil/water separation, J. Mater. Chem. A 9 (2021) 21659–21684, https://doi.org/10.1039/D1TA05873H.

[22] H. Song, L. Xu, M. Chen, Y. Cui, C. Wu, J. Qiu, L. Xu, G. Cheng, X. Hu, Recent progresses in the synthesis of MnO2 nanowire and its application in environmental catalysis, RSC Adv. 11 (2021) 35494–35513, https://doi.org/10.1039/D1RA06497E.

[23] T.-H. Wu, Y.-Q. Lin, Z.D. Althouse, N. Liu, Dissolution-redeposition mechanism of the MnO2 Cathode in aqueous zinc-ion batteries, ACS Appl. Energy Mater. 4 (2021) 12267–12274, https://doi.org/10.1021/acsaem.1c02064.

[24] J. Yuan, X. Liu, O. Akbulut, J. Hu, S.L. Suib, J. Kong, F. Stellacci, Superwetting nanowire membranes for selective absorption, Nat Nanotechnol 3 (2008) 332–336, https://doi.org/10.1038/nnano.2008.136.

[25] X. Yue, T. Zhang, D. Yang, F. Qiu, Z. Li, Ultralong MnO2 nanowire enhanced multiwall carbon nanotube hybrid membrane with underwater superoleophobicity for efficient oil-in-water emulsions separation, Ind. Eng. Chem. Res. 57 (2018) 10439–10447, https://doi.org/10.1021/acs.iecr.8b02577.

[26] S. Sau, S. Pandit, S. Kundu, Crosslinked poly (vinyl alcohol): structural, optical and mechanical properties, Surf. Interfaces 25 (2021) 101198, https://doi.org/10.1016/j.surfin.2021.101198.

[27] N.M.A. Omar, M.H.D. Othman, Z.S. Tai, M. Milad, M.N.M. Sokri, M.H. Puteh, Recent progress and technical improvement strategies for mitigating ceramic membrane bottlenecks in water purification processes: a review, Int. J. Appl. Ceram. Technol. 20 (2023) 3327–3356, https://doi.org/10.1111/ijac.14503.

[28] N.M.A. Omar, M.H.D. Othman, Z.S. Tai, T.A. Kurniawan, T. El-badawy, P.S. Goh, N.H. Othman, M.A. Rahman, J. Jaafar, A.F. Ismail, Bottlenecks and recent improvement strategies of ceramic membranes in membrane distillation applications: a review, J. Eur. Ceram. Soc. 42 (2022) 5179–5194, https://doi.org/10.1016/j.jeurceramsoc.2022.06.019.

[29] G. Pećanac, S. Foghmoes, M. Lipińska-Chwałek, S. Baumann, T. Beck, J. Malzbender, Strength degradation and failure limits of dense and porous ceramic membrane materials, J. Eur. Ceram. Soc. 33 (2013) 2689–2698, https://doi.org/10.1016/j.jeurceramsoc.2013.04.018.

[30] N. Nagendra, R.F. Klie, N.D. Browning, S. Bandhopadhyay, Fracture characterization in tubular LSFCO ceramic membranes, Mater. Sci. Eng. A 341 (2003) 236–246, https://doi.org/10.1016/S0921-5093(02)00242-3.

[31] T. Takashima, K. Hashimoto, R. Nakamura, Mechanisms of pH-dependent activity for water oxidation to molecular oxygen by MnO2 electrocatalysts, J. Am. Chem. Soc. 134 (2012) 1519–1527, https://doi.org/10.1021/ja206511w.